Magnetic-field-induced V-shaped quantized conductance staircase in a double-layer quantum point contact

S. K. Lyo
Sandia National Laboratories, Albuquerque, New Mexico 87185
(Received 12 January 1999)

We show that the low-temperature conductance (G) of a quantum point contact consisting of ballistic tunnel-coupled double-layer quantum-well wires is modulated by an in-layer magnetic field B due to the anticrossing. B creates a V-shaped quantum staircase for G, causing it to decrease in steps of $2e^2/h$ to a minimum and then increase to a maximum, where G may saturate or decrease again at higher B's. Relevance of the result to recent data is discussed. [S0163-1829(99)14935-X]

The low-temperature conductance (G) through a narrow constricted channel known as a quantum point contact is quantized in units of $2e^2/h$.[1] This quantization follows from the fact that, in one dimension, each pair of Fermi points on an energy-dispersion curve of a sublevel contributes e^2/h per spin σ to $G=(e^2/h)\Sigma_\sigma \nu_{F\sigma}$, independent of the form of the dispersion. Here $\nu_{F\sigma}$ is the number of pairs of Fermi points $\nu_{F\sigma}$.[1]

We consider a quantum point contact consisting of coupled double quantum wells (DQW's) separated by a thin barrier shown in Fig. 1. The confinement in the z direction yields sublevels which will be referred to here as *QW sublevels*. The QW widths w_1, w_2 and the center-to-center distance d are small, allowing only the tunnel-split ground doublet to be occupied: higher QW sublevels are *not* considered explicitly except that they enhance the mass of the electrons of the ground doublet through sublevel mixing at high fields B. The channel is a few tenths of a micron wide, yielding densely spaced sublevels arising from the confinement in the x direction. These dense sublevels are defined as *channel sublevels* or simply as *sublevels*. The current flows *ballistically* along the channel. The purpose of this paper is to show that $B(\|\mathbf{x})$ creates a V-shaped staircase of the quantized $G(B)$ by causing G to decrease initially to a minimum value in steps of $2e^2/h$ in a system with a small g factor and then to increase to a maximum value. For narrow (wide) QW's, G saturates (decreases again) at higher B's and the saturation (maximum) G is larger (smaller) than $G(B=0)$. A similar behavior was observed recently. A single-QW quantum point contact with $B\|\mathbf{z}$ has been studied earlier. In this case, G decreases monotonically with increasing B in steps of $2e^2/h$.[1,2]

The wave function for the structure shown in Fig. 1 is given by $\Psi = e^{ik_y y}\phi_n(x)\psi(z,k_y)$, where n indicates the channel sublevels. The wave function $\phi_n(x)$ is determined by the shape of the channel confinement potential and is treated here phenomenologically. The DQW eigenfunction for the z confinement $\psi(z,k_y)$ is determined by

$$H = -\frac{\hbar^2}{2}\frac{\partial}{\partial z}\frac{1}{m^*}\frac{\partial}{\partial z} + \frac{\hbar^2}{2m^*}\left(k_y - \frac{z}{l^2}\right)^2 + V(z) + \varepsilon_n + \sigma g \mu_B B, \quad (1)$$

where ε_n is the sublevel energy, $l=(\hbar c/eB)^{1/2}$, and $V(z)$ is the double-well potential illustrated in Fig. 1. The last term is the Zeeman energy where μ_B is the Bohr magneton and $\sigma=0,1$. The effect of the Zeeman splitting is negligibly small for GaAs QW's with $g=0.44$. The Hamiltonian in Eq. (1) with $\varepsilon_n=\hbar^2 k_x^2/2m^{*2}$ has been studied earlier[3] and explains many interesting phenomena in *two-dimensional* DQW's including the magnetoresistance,[3–6] anomalous cyclotron mass,[7–9] and the conductance enhancement in DQW wires with a short mean free path.[10]

We solve Eq. (1) numerically by transforming it into a three-point difference equation. Two symmetric (sy1,sy2) and two asymmetric (asy1,asy2) $GaAs/Al_{0.3}Ga_{0.7}As$ DQW structures, listed in Table I, are studied. Figure 2(a) shows the $B=0$ eigenvalues of Eq. (1) for the symmetric and antisymmetric ground doublet of sy1 including five low-lying sublevels evenly spaced at energy intervals of $\delta=0.02$ meV. The effective mass is $m^*=0.067$ in the QW's and $m^*=0.091$ in the barriers in units of the free-electron mass. The vertical dots signify an infinite stack of the sublevels.

For $B>0$, we turn off interwell tunneling initially. The confinement wave functions are then centered at $z=\mp d/2$. The effective wave numbers $\tilde{k}_y = k_y - z/l^2 = k_y \pm d/2l^2$ in the second term of Eq. (1) for the left and right QW's are shifted relative to each other by an amount $\Delta k_y = d/l^2$. The two shifted energy-dispersion parabolas intersect each other at $k_y=0$. The degeneracy at the crossing point is removed by interwell tunneling, yielding an anticrossing gap which separates the lower branch from the upper branch as shown in Fig. 2(b) at $B=2.7$ T. A *hump* is formed at the lower gap edge only at a sufficiently high B. In Fig. 2(c), the gap (not shown) lies far above the chemical potential (μ) shown by

TABLE I. DQW's with well widths w, center-barrier width t, well depths V_1, V_2, and $B=0$ energy gap Δ_0.

Structure	w/t (Å)	V_1/V_2 (meV)	Δ_0 (meV)
sy1	150/25	280/280	1.39
sy2	135/40	280/280	0.55
asy1	150/25	280/279	1.71
asy2	200/20	280/279	1.46

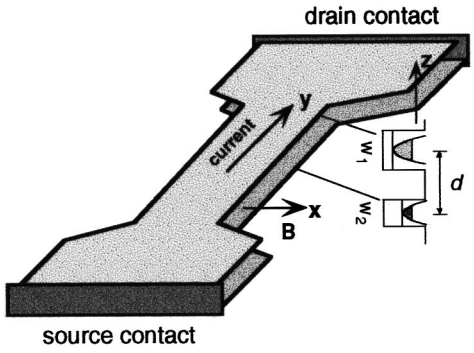

FIG. 1. A bilayer quantum point contact. The field B ($\|\mathbf{x}$) is perpendicular to both the channel ($\|\mathbf{y}$) and the growth direction (z). Here, $d \ll$ channel width.

thick horizontal bars for $N=2.0\times10^7\,\mathrm{cm}^{-1}$. Note that B deforms the dispersion curve from Fig. 2(a) to Fig. 2(b) by stretching out the lower branch in the k_y direction, introducing additional extrema and large (e.g., divergent) densities of states. This process transfers states from the upper branch to the region below the gap, thereby lowering μ toward the bottom of the lower branch. This important point is clearly seen in Figs. 2(a) and 2(b), where μ decreases from 1.64 at $B=0$ T to 1.05 meV at $B=2.7$ T (relative to the bottom of the lower branch). As a result, significantly fewer sublevels are necessary to accommodate the electrons at $B=2.7$ T, reducing the number of Fermi points and thus G.

With further increasing B, the lower gap edges rise, crossing μ, and doubling the number of Fermi points from two to four for each crossed hump and thereby increasing G steadily to a maximum. At high B's, G saturates as the two groups of the parabolas become separated as shown in Fig. 2(c). For DQW's with very wide wells, however, G decreases again at higher B's due to the mass enhancement caused by B-induced mixing of the QW sublevels, as will be shown later.

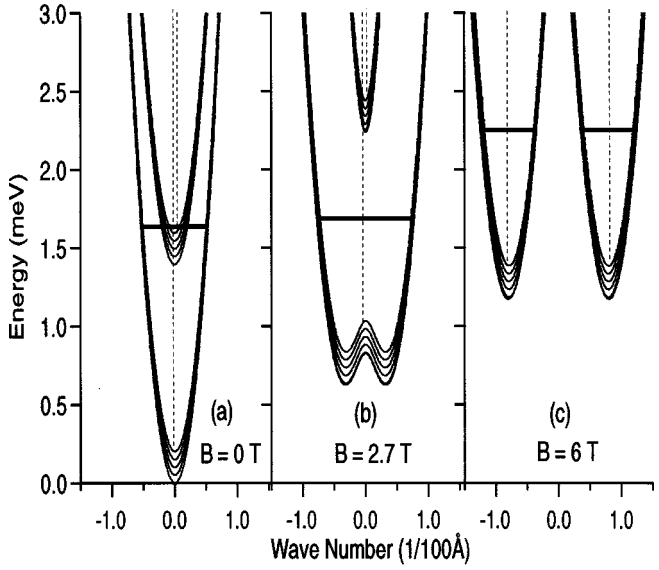

FIG. 2. Energy-dispersion curves for sy1 with five low-lying channel sublevels spaced at $\delta=0.02$ meV (not to the scale). The dotted lines signify higher sublevels. The horizontal bars denote the chemical potential μ for $N=2.0\times10^7\,\mathrm{cm}^{-1}$.

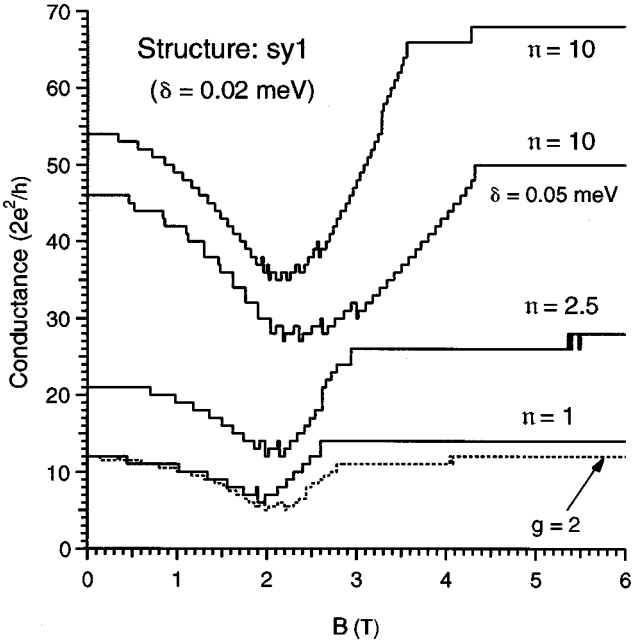

FIG. 3. Conductance as a function of B for sy1. The dotted curve shows the effect of spin splitting for $g=2$.

The B-dependent G is displayed in Fig. 3 for sy1 for several electron densities $N\equiv n\times10^6\,\mathrm{cm}^{-1}$ and $\delta=0.02$ and 0.05 meV. For the same δ, the reduction $\Delta G=G(B=0)-G(B=B_{\min})$ at the G minimum at $B=B_{\min}$ is larger for a larger n. This is readily understood from the fact that, for a larger N, μ is larger, populating a larger number of sublevels, yielding a larger initial $G(B=0)$. Also, it takes a larger B to pass the hump through μ, yielding a larger $B_{\min}$. In this process, a larger number of the sublevels are emptied, resulting in a larger ΔG at $B=B_{\min}$. For the two curves with $\delta=0.05$ and 0.02 meV with the same $n=10$, $B_{\min}$ is larger for a larger δ because μ is larger for a larger δ. The dotted curve shows the effect of spin splitting for $g=2$. The effect is negligible for $g=0.44$. For $n=20$ (cf. Fig. 2), G is similar to that for $n=10$ but is larger.

Figure 4 compares G for sy2, asy1, and asy2 for $\delta=0.02$ meV. The $B=0$ energy gap Δ_0 of sy2 is smaller than that of sy1, yielding a smaller $\mu=0.92$ meV compared to $\mu=1.07$ meV of sy1 for $n=10$. In sy1, the occupied sublevels consist of only the lower branch of the QW doublet because $\mu<\Delta_0$. The sublevels just under the Fermi level are a rich source of Fermi points without adding many occupied states. For sy2, with $\mu>\Delta_0$, there are two stacks of occupied sublevels, each consisting of the lower and the upper branch, thereby providing two rich sources of Fermi points and yielding a larger $G(0)$ than sy1. For sy2, both $B_{\min}$ and the relative drop of G at $B_{\min}$ are smaller than those of sy1 because the hump passes through μ at a lower B.

For the asymmetric structure asy1, $\Delta_0=1.71$ meV includes the 1.0-meV energy mismatch and is larger than $\Delta_0=1.39$ meV of sy1. The $G(B_{\min})$ is shallow and occurs at a $B_{\min}$, which is somewhat higher than that of sy1. Note that, in asymmetric DQW's, the two noninteracting parabolas intersect twice as they are displaced by B: the first time, with the same sign of the slopes, and the second time, with opposite signs. The hump develops at the lower gap edge at the

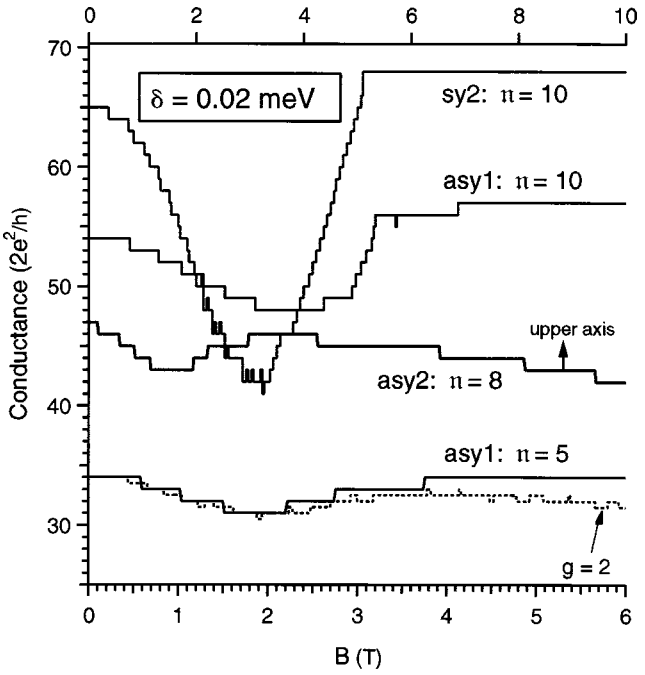

FIG. 4. Conductance as a function of B for structures sy2, asy1, and asy2 (upper scale). The dotted curve shows the effect of spin splitting for $g=2$.

higher B (e.g., $B=2.9\,\mathrm{T}$) when the two parabolas intersect with opposite signs of the slopes, yielding a higher $B_{\min}$. The spin splitting is also shown in Fig. 4 for $g=2$ (dotted curve). Recently, the G-minimum behavior shown in Figs. 3 and 4 with a similar order of magnitude, but with the quantum steps unresolved, has been observed at $T=0.3\,\mathrm{K}$.[11] The quantum steps are smeared out for $k_BT \gtrsim \delta$.

The ratios $R \equiv G(\infty)/G(0)$ saturate at large $B \equiv B_\infty$ for most of the curves in Figs. 3 and 4. The asymptotic behavior of $G(B_\infty) \equiv G_\infty$ is reached when μ is far below the gap as in Fig. 2(c). In DQW's with deep narrow QW's (e.g., sy1, sy2, and asy1) with negligible mixing of QW sublevels, a larger B merely displaces the parabolas further away without changing their shapes, μ, or G. While most of the R's in Figs. 3 and 4 are larger than unity, R is less than unity for the bottom curve (with $g=2$) and the asy2 curve in Fig. 4. For the latter, R decreases after reaching a maximum. These anomalies are due to a combination of large Zeeman splitting, field-induced mass enhancement, and the energy asymmetry ΔE (without tunneling), as will be shown below.

We find, equating the number of the occupied states at $B=0\,\mathrm{T}$ and $B=B_\infty$,

$$2\sqrt{1-\gamma}\sum_{n=0}^{\infty}\sum_{\sigma'=0,1}\sqrt{\mu_0-\sigma'\Delta_0-\varepsilon_n} = \sum_{n=0}^{\infty}\sum_{\sigma,\sigma'=0,1}\sqrt{\mu_\infty-(\sigma'\Delta E+\varepsilon_n+\sigma g\mu_B B_\infty)}. \tag{2}$$

Here the square roots vanish for negative arguments and μ_0, μ_∞ are μ's at $B=0$ and $B \equiv B_\infty$. $1-\gamma$ is the ratio of the mass along the channel at $B=0$ and $B \equiv B_\infty$ in the QW's.

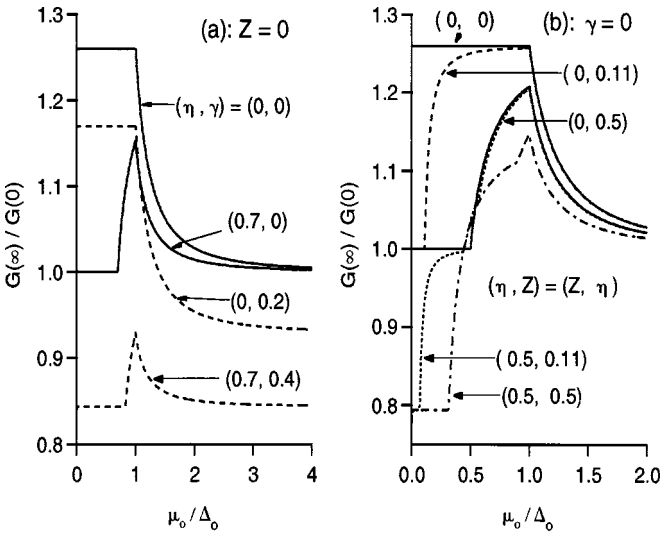

FIG. 5. Conductance ratio R vs μ_0/Δ_0 (defined in the text) for uniformly spaced channel sublevels in the absence of (a) the Zeeman splitting and (b) the mass enhancement.

For $\varepsilon_n = n^\alpha \delta$ ($\alpha=1,2$) with $\delta \ll \mu_0, \mu_\infty$, the n summation in Eq. (2) yields

$$2\sqrt{1-\gamma}\sum_{\sigma'=0,1}(x-\sigma')^{2-0.5\alpha}\theta(x-\sigma') = \sum_{\sigma'=0,1}\sum_{\sigma=0,1}(y-\sigma\eta-\sigma' Z)^{2-0.5\alpha}\theta(y-\sigma\eta-\sigma' Z), \tag{3}$$

where $x=\mu_0/\Delta_0$, $y=\mu_\infty/\Delta_0$, $\eta=\Delta E/\Delta_0$, $Z=g\mu_B B_\infty/\Delta_0$, and $\theta(x)$ is a unit step function. The ratio R then equals

$$G(\infty)/G(0) = \frac{\sum_{\sigma'=0,1}\sum_{\sigma=0,1}(y-\sigma\eta-\sigma' Z)^{1.5-0.5\alpha}\theta(y-\sigma\eta-\sigma' Z)}{2\sum_{\sigma'=0,1}(x-\sigma')^{1.5-0.5\alpha}\theta(x-\sigma')}. \tag{4}$$

The quantity R is plotted as a function of $x=\mu_0/\Delta_0$ in Fig. 5 for $\varepsilon_n = n\delta$. For $Z=0$ and $\gamma=0$, $R \geqq 1$ as seen from Fig. 5(a) and is consistent with the results in Fig. 3. For symmetric DQW's (i.e., $\eta=0$), R equals $2^{1/3}=1.26$ and $\sqrt{2}=1.41$, respectively, for $\alpha=1$ and 2 in the region $x \leqq 1$ and decreases monotonically above $x>1$, approaching unity at large x. For asymmetric DQW's (i.e., $\eta>0$) with $\gamma=0$, R equals unity for $x \leqq \eta$, increases monotonically to a maximum at $x=1$, and decreases monotonically approaching unity at large x.

We estimate $\gamma \approx 2\hbar\omega_c\langle 1|z|2\rangle^2/(E_{12}^* l^2)$ for single-well QW sublevels $|1\rangle$ and $|2\rangle$ with parity. Here $\hbar\omega_c$ is the cyclotron energy and $E_{12}^* = E_{12} + \hbar\omega_c(\langle 2|z^2|2\rangle - \langle 1|z^2|1\rangle)/2l^2$ is the level separation. A similar effect was found earlier using a different approach.[12] The quantity γ increases the density

of states, reducing the number of occupied sublevels and thus R, as shown by the dashed curves in Fig. 5(a). This effect is important in wide QW's such as asy2, where $\gamma=0.09$ at 10 T due to B-induced mixing of the QW sublevels. For the asy2 curve in Fig. 4 with $x=0.63$ and $\eta=0.68$, R is smaller than unity, as shown in Fig. 5(a): γ increases with B, yielding a maximum in G.

For $Z>0$, R is invariant under the interchange $\eta \leftrightarrow Z$. The effect of Z is shown in Fig. 5(b), where $Z=0.11$ and 0.5 correspond, respectively, to the spin splitting at $B_\infty=6$ T for $g=0.44$, $g=2$, and $\Delta_0=1.39$ meV. An interesting aspect of the result in Fig. 5(b) is that, when x is less than the lesser of (η,Z) times $2^{-2/3}$, R equals $R=2^{-1/3}$, which is about 20% less than unity.

The conductance displayed in Figs. 3 and 4 is consistent with the results shown in Fig. 5. The G ratios obtained from the curves with $n=10$ in Figs. 3 and 4 agree with those from Fig. 5(a). For the low-density case $n=2.5$ in Fig. 3, however, R shows a 5% deviation from the theoretical value in Fig. 5(a) because the continuum approximation is poor at low densities. The effect of spin splitting on G in Figs. 3 and 4 is small for GaAs QW's. However, for $g=2$, the effect is significant at high B's. An interesting aspect of the Zeeman splitting occurs when it is combined with the asymmetry $\eta>0$. In this case, R can become less than 1 as shown in Fig. 5(b) and occurs for the bottom curve in Fig. 4.

For large δ, fewer sublevels are populated, yielding a smaller G as seen in Fig. 3. The δ dependence of G is displayed in Fig. 6 for sy1 for $B=0$, 2.2, and 6 T. The dashed curves there represent the analytic results obtained from the continuum approximation. Here, G drops as $\delta^{-1/3}$ for small $\delta<0.12$ meV.

In summary, we have shown that a perpendicular B creates a V-shaped quantized conductance staircase for a DQW quantum point contact, decreasing G to a minimum in steps of $2e^2/h$ and then increasing it to a maximum, where G saturates (decreases again) for narrow (wide) QW's at higher B's. The effect of B-induced mass enhancement and spin splitting was examined.

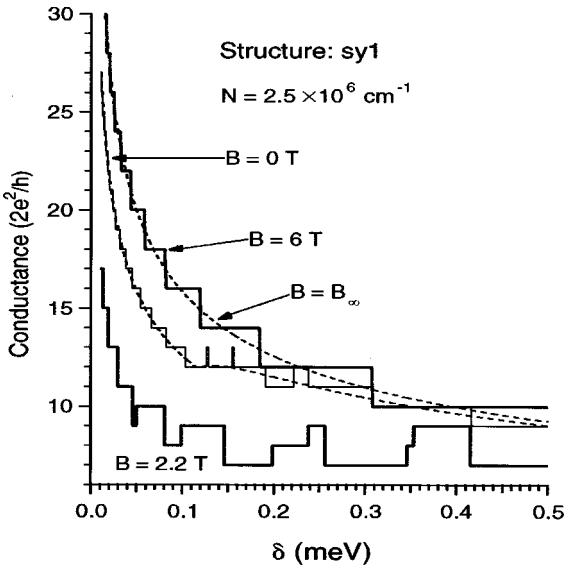

FIG. 6. Conductance vs the uniform sublevel spacing for sy1 and $g=0$. The dashed curves are the continuum results without mass enhancement (i.e., $\gamma=0$) at $B=0$ and at asymptotic fields $B=B_\infty$.

The author thanks J. S. Moon, J. A. Simmons, and M. Blount for the discussions about the double quantum wire structures and for making their data available to him prior to publication. Sandia is a multiprogram laboratory operated by Sandia Corporation, a Lockheed Martin Company, for the U.S. DOE under Contract No. DE-AC04-94AL85000.

[1] C. V. J. Beenaker and H. van Houton, in *Solid State Physics: Semiconductor Heterostructures and Nanostructures*, edited by H. Ehrenreich and D. Turnbull (Academic, New York, 1991), Vol. 44, and references therein.
[2] B. J. van Wees *et al.*, Phys. Rev. B **38**, 3625 (1988).
[3] S. K. Lyo, Phys. Rev. B **50**, 4965 (1994).
[4] J. A. Simmons, S. K. Lyo, N. E. Harff, and J. F. Klem, Phys. Rev. Lett. **73**, 2256 (1994).
[5] A. Kurobe *et al.*, Phys. Rev. B **50**, 4889 (1994).
[6] O. E. Raichev and F. T. Vasko, Phys. Rev. B **53**, 1522 (1996).
[7] J. A. Simmons, N. E. Harff, and J. F. Klem, Phys. Rev. B **51**, 11 156 (1995).
[8] S. K. Lyo, Phys. Rev. B **51**, 11 160 (1995).
[9] I. S. Millard *et al.*, J. Phys.: Condens. Matter **9**, 1079 (1997).
[10] S. K. Lyo, J. Phys.: Condens. Matter **8**, L703 (1996).
[11] J. S. Moon *et al.* (unpublished); S. T. Stoddart *et al.* (unpublished).
[12] L. Smrcka and T. Jungwirth, J. Phys.: Condens. Matter **6**, 55 (1994).